Collective plasma effects of electron–positron pairs in beam-driven QED cascades

F SCI

iD Kenan Qu, iD Sebastian Meuren and iD Nathaniel J. Fisch

COLLECTIONS

F   This paper was selected as Featured

SCI   This paper was selected as Scilight

View Online   Export Citation   CrossMark

Collective plasma effects of electron–positron pairs in beam-driven QED cascades 🔵 🔵

Kenan Qu,[1,a)] 🔵 Sebastian Meuren,[1,2] 🔵 and Nathaniel J. Fisch[1] 🔵

AFFILIATIONS

[1]Department of Astrophysical Sciences, Princeton University, Princeton, New Jersey 08544, USA
[2]Stanford PULSE Institute, SLAC National Accelerator Laboratory, Menlo Park, California 94025, USA

a)Author to whom correspondence should be addressed: kq@princeton.edu

ABSTRACT

Understanding the interplay of strong-field QED and collective plasma effects is important for explaining extreme astrophysical environments like magnetars. It has been shown that QED pair plasma can be produced and observed by passing a relativistic electron beam through an intense laser field. This paper presents in detail multiple sets of 3D QED-particle-in-cell simulations to show the creation of pair plasma in the QED cascade. The beam driven method enables a high pair particle density and also a low particle Lorentz factor, which both play equal roles on exhibiting large collective plasma effects. Finite laser frequency upshift is observed with both ideal parameters (24 PW laser colliding with a 300 GeV electron beam) and with existing technologies (3 PW laser colliding with a 30 GeV electron beam).

Published under an exclusive license by AIP Publishing. https://doi.org/10.1063/5.0078969

I. INTRODUCTION

When the Schwinger field[1] is greatly exceeded, it is possible to reach the so-called QED plasma regime, which exhibits both strong-field quantum effects and collective plasma effects. The QED plasma regime is characterized by both high field strength to produce pairs and relatively high pair density to exhibit the collective effects. Above the QED critical limit 10^{18} Vm^{-1}, photons and electron–positron pairs are created in a cascaded manner.[2–13] The resultant pairs travel at relativistic speeds, usually with high Lorentz factor.

This extreme regime is reached in intriguing astrophysical environments like magnetars,[14,15] binary neutron-star mergers,[16,17] and core-collapse supernovae explosions.[18,19] For example, magnetars[20–24] are filled with strong-field QED cascades of relativistic electron–positron pair plasma[25–28] in their magnetospheres. The relativistic particle emission in the varying magnetic field of magnetars is very likely responsible for the fast radio bursts.[29–32] It often turns out to be of paramount importance[33–35] to appreciate the collective plasma effects in these extreme environments.[36–40]

To describe these collective effects, it might be surmised that the full machinery of collective plasma effects can simply be carried over to the QED pair-plasma regime. It also might be surmised that, if the dynamics underlying these collective effects can be considered understood, then there would be few surprises in predicting collective phenomena. However, without probing this regime in laboratory experiments, there cannot really be surety that there will be no such

surprises. After all, a pair plasma, created out of extreme field energy, and constantly subject to both creation and recombination, is an exotic state of matter. Can we be sure that the created particles obey the same collective effects found in less exotic plasmas? It behooves us to check experimentally the theoretical expectations and simplifications. Hence, given the high interest in this regime, and given the high intensity lasers that are now available, it is now both critical and timely to perform the laboratory experiments that might exhibit the expected QED collective effects.

However, realizing the QED plasma regime—and probing its collective effects—while technically possible, is not so simple. QED plasma dynamics have been explored theoretically.[41–62] Possibilities for creating the QED regime in laboratory experiments have also been explored.[63–75] Note that the particle density necessary to manifest collective plasma effects depends on the observation method. One way is to measure the wavelength of the plasma emission driven by a laser field. To emit at an infrared wavelength (to which the detectors are most sensitive), the particle density needs to reach near 10^{25}–10^{27} m^{-3}. This corresponds to a 0.001–0.1 nC pair plasma in a 1 μm^{-3} volume sphere.

The all-optical approach to reaching and observing the QED regime employs two colliding ultra-strong lasers. Strong beat wave accelerates seed electrons to relativistic speeds, which in turn boosts the laser field amplitude. As soon as the QED critical field is reached in the electron rest frame, high energy photons are emitted and pairs

are created. The strong laser continues to accelerate the particles to induce a QED cascade. With a sufficiently strong laser field, a QED cascade is produced in the rest frame of the pair particles leading to a pair plasma. It was proposed[63] that laser intensities above 10^{24} Wcm^{-2} are sufficient to probe the QED critical field in the pair particle rest frame. This all-optical method has prompted investigation both analytically and numerically.[63–74] However, the 10^{24} Wcm^{-2} laser intensity required by the all-optical method needs a technologically challenging tight focus of a 100 PW laser.[76–78] Solving this challenge will depend on substantial development beyond current state-of-the-art laser technology. Even if the pair plasma is created, the pair particles have a large Lorentz factor of $\sim 10^3$. The large Lorentz factor is important, since the pairs contribute to the plasma frequency (observed in the laboratory frame) inversely to their relativistic mass. The smallness of this contribution means that even higher densities of pairs are necessary to make substantive contributions to collective plasma effects.

Here, we describe an alternative, less technologically challenging than the all-optical approach to reaching the QED plasma regime by colliding a less intense laser pulse with an electron beam. The idea, introduced recently[75] and expanded upon here, is to generate a quasi-neutral pair-plasma with a density that is comparable to the critical one by using the combination of a 30 PW laser and a dense 300 GeV electron beam or by using less stringent parameters. This method circumvents the technological limitations by taking advantage of the high quality energetic electron beam facilities to boost the laser intensity in the particle rest frame. It also facilitates observation of the QED collective effects, since in the end, what must be solved is not merely reaching the QED plasma regime, but reaching the QED plasma regime and observing its collective effects. Hence, what must be optimized is the joint production-observation problem. If the pairs produced are less energetic, then, at much lower pair densities, there can be larger, more easily observed, contributions to collective effects.

This paper is organized as follows: In Sec. II, we briefly outline why the beam–laser approach directly engages the joint production-observation problem. In Sec. III, in order to provide context for our numerical simulations, we review the physics of the QED cascade in an electron beam–laser collision. In Sec. IV, we introduce the setup of our 3D particle-in-cell (PIC) QED simulations and show the production of electron–positron pairs. In Sec. V, we focus on the pair deceleration through both synchrotron emission and laser radiation pressure. The important pair reflection condition is introduced here. In Sec. VI, we analyze the laser dynamics and show how its spectrum changes with the increasing plasma frequency. Multiple optical detection methods are explained, including laser central frequency shift, chirping, and homodyne detection of the laser phases. In Sec. VII, we verify the scaling of the laser frequency shift with different electron beam and laser parameters. In Sec. VIII, we demonstrate the possibility of creating and observing a QED plasma using state-of-the-art parameters, i.e., a 3 PW laser and a dense 30 GeV electron beam (through, for example, a combination of FACET-II with LCLS-Cu RF LINAC[79]). In Sec. IX, we present our conclusions.

II. BEAM-LASER APPROACH TO THE PRODUCTION-OBSERVATION PROBLEM

Consider the rest frame of high energy particle beams, because reaching the Schwinger field limit directly in laboratories is still beyond the capability of current technology. A multi-GeV electron beam from a particle accelerator can have a Lorentz factor of over 10^4, which can boost the laser field by the same number. The seminal SLAC E-144 experiment[80,81] has already used this method to observe evidence of nonlinear Compton scattering and Breit–Wheeler pair production by colliding a $\sim 10^{18}$ Wcm^{-2} laser and a ~ 50 GeV electron beam. Due to the relatively low laser intensity, only a limited number of positrons were produced, so that collective plasma effects could not be observed. The upcoming experiment SLAC FACET-II will deploy a new laser with over 10^{20} Wcm^{-2} peak intensity. Combined with the LCLS-Cu LINAC,[82–84] a pair multiplication factor over unity can be achieved providing a unique opportunity to explore the QED pair plasma.

Compared with the all-optical method, the beam-driven approach lowers the laser intensity requirement by two orders of magnitude. This is because particle accelerators can produce multi-GeV or even tens of GeV electron beam energy, corresponding to Lorentz factor of 10^4–10^5. A PW-level laser can already induce QED pair multiplication. Such laser systems are routinely operated in several laboratories.[78] The all-optical method only accelerates the electrons to a Lorentz factor similar to the laser dimensionless amplitude a; even reaching $\gamma \sim 10^3$ needs laser intensity of over 10^{24} Wcm^{-2}[63–74] and, thus, requires large 100 PW-scale laser facilities.[76–78]

As the pair density grows in a QED cascade, collective plasma effects emerge. Existing experimental detectors, like magnetic spectrometers, can distinguish electrons and positrons but cannot measure the pair density or observe a collective plasma effect. The figure of merit for collective plasma dynamics is determined by the plasma frequency (ω_p), which is proportional to the ratio of pair particle density (n_p) and pair Lorentz factor (γ), i.e., $\omega_p \propto \sqrt{n_p/\gamma}$. Since the average pair Lorentz factor is similar to the laser dimensionless amplitude, the lower laser intensity needed for the beam-driven approach greatly reduces the average Lorentz factor of the produced pair plasma. It, thus, exhibits higher plasma frequency even if the colliding lasers can produce the same plasma density. The counterpropagating configuration of the laser pulse and pairs also further slows down the pairs through laser radiation pressure. Thus, the pair plasma created in a beam-driven QED cascade is easier to detect than one created with the all-optical approach. All of these advantages, favoring the beam-driven approach over the all-optical approach, accrue from the simple fact that the pair masses, and hence, their contributions to the pair plasma frequency are inversely proportional to the pair Lorentz factor.

There are further advantages to the beam-driven approach. The laser, which is used to create pair plasma, also informs the pair plasma property through its change in spectrum. Both as the pair plasma forms and as it slows down, the plasma frequency increases inside laser field. The increase in plasma frequency abruptly reduces the vacuum refractive index, which mediates the laser. The consequence is that laser frequency is upshifted and the laser wavelength is blue shifted, according to the theory of temporal change in optical refractive index.[85–94] The optical emission, thus, serves as a robust signature of the creation of collective plasma effects in the QED plasma despite the small plasma volume and relativistic plasma motion. In fact, the small plasma volume (μm-scale) eliminates the possibility of using conventional detection methods, e.g., by observing plasma instabilities, like the two-stream instability,[95] the Weibel instability,[96] or stimulated Brillouin scattering (SBS).[97]

III. PAIR GENERATION THROUGH BEAM-DRIVEN QED CASCADE

To give context to numerical simulations that support the beam-driven approach, we provide first a brief overview of the QED cascade process. In an electron beam-driven QED cascade, an energetic electron beam collides with a counter-propagating strong laser field. The laser amplitude is greatly boosted to exceed the critical field E_s in the electron rest frame. Thus, the electrons emit photons, which further split into electron–positron pairs. Each of the pair particles, given sufficient energy, continues the photon emission and pair generation process to induce a cascaded generation of pairs. The process converts high electron beam energy into large pair numbers. In this section, we lay out the properties of beam-driven QED cascade while we briefly explain how the electron–positron pairs are generated.

In the initial stage of the collision, the electron beam has the maximum energy with a Lorentz factor γ. It boosts the counter-propagating laser field by the same factor γ in the rest frame of the electrons. Such a boost aims to produce a large quantum parameter for electrons $\chi_e \equiv E^*/E_s = \gamma|\mathbf{E}_\perp + \boldsymbol{\beta} \times c\mathbf{B}|/E_s$, where $\mathbf{E}$ and $\mathbf{B}$ are the electric and magnetic field of the laser in the laboratory frame and β is the electron beam speed normalized to the speed of light c. The strong laser field drives electron motion, causing emission of photons.[2,98]

The photon emission spectra differ depending on the quantum parameter χ_e. The regime $\chi_e \gtrsim 1$ is reached near the laser intensity peaks where quantum synchrotron emission causes an electron to emit almost all of its energy into a single gamma ray. In the regions of low laser intensity $\chi_e \ll 1$, the emission is classical, and the emitted photon $\hbar\omega$ only takes a small portion of the electron energy $\mathcal{E}$, i.e., $\hbar\omega \sim \chi_e\mathcal{E}$.

The low energy photons would escape laser focus spot without decaying into pairs, but high-energy gamma ray photons are highly likely to decay into an electron–positron pair in the same strong laser field. For the interest of this paper, we focus on the Breit–Wheeler process that a photon decays into one pair of electron and positron. The decaying process depends on the quantum parameter of the emitted photon $\chi_\gamma \equiv [\hbar\omega/(2m_ec^2)]|\mathbf{E}_\perp + \hat{\mathbf{k}} \times c\mathbf{B}|/E_s$, where $\hbar\omega(\hbar\mathbf{k})$ is the photon energy (momentum) and m_e is the electron rest mass. The pair generation happens only when χ_γ is above the unit threshold value. For $\chi_\gamma \gg 1$, the photon transfers almost all of its energy to either the electron or positron, while for smaller χ_γ values, the photon energy is more symmetrically partitioned.

Therefore, a very intense laser can cause a cascade of gamma rays and pairs from a single energetic electron. Each subsequent emission and decay process transfers energy predominantly into one new particle and creates many other particles with lower energies. The total energy of pairs and photons is conserved, which allows us to find the pair number multiplication factor. Combined with the fact that the gamma photon decay process terminates when $\chi_\gamma < 1$, the pair number grows by a factor that is approximately equal to the maximum quantum factor χ_e at the laser peak amplitude. Thus, for an electron beam with original Lorentz factor γ_0 and density n_e and a laser with dimensionless amplitude $a_0 \equiv eE/(m_ec^2\omega_0)$ and frequency ω_0, the pair number multiplies as

$$n_p \sim \tilde{\chi}_e n_e, \quad \tilde{\chi}_e \approx 2a_0\gamma_0(\hbar\omega_0)/(m_ec^2). \quad (1)$$

This relation holds only if the laser pulse is sufficiently wide and long. Finite laser pulse waist and duration could cause deviation of the pair multiplication factor from the estimation, but the linear scaling should nevertheless hold in general. It should be born in mind that the quantum parameter for the pairs χ_e and for the photons χ_γ depend on the local laser field strength, and hence, they vary at a different location and time. The pair number multiplication factor $\tilde{\chi}_e$ is approximately equal to the maximum quantum parameter for the pairs and, hence, is a fixed value for certain laser pulse and electron beam energy.

The quantum photon emission process has a lower requirement for the field and it terminates when $\chi_e \ll 1$. Though the relatively low energy photons do not decay into pairs, they play an important role in decelerating the pair particles, which contributes to higher collective plasma effects.

Since the pair formation rate $t_f^{-1} \sim 2a_0\omega_0$ is proportional to the laser amplitude $a_0(\gg 1)$, the pairs are more likely to be created in the region where the laser field is strong. The strong laser field drives pair oscillation immediately when they are generated. The collective effects, if they were to be probed, are manifested through the oscillation of the pair particles in the strong laser field.

IV. 3D PIC QED SIMULATIONS OF PAIR CREATION

The above analysis shows that an electron beam-driven QED cascade requires an intense laser field with $a_0 \gg 1$ and an electron beam with high γ factor such that $\chi_e \gtrsim 1$. Toward this limit, our simulations consider head-on collision of a 1 nC electron beam of 300 GeV,[99,100] shown as a blue sphere in Fig. 1, and a 24 PW laser pulse[77] with wavelength $\lambda = 0.8\,\mu m$, shown as an yellow spheroid. The corresponding dimensionless laser amplitude is $a_0 \approx 170$, and the maximum quantum parameter is $\tilde{\chi}_e \approx 220$ at the Gaussian waist in the focal plane, and $\tilde{\chi}_e \approx 600$ at the laser focus.

The electron beam has a spherical Gaussian number density $n_e(\mathbf{r}) = n_{e0}\exp[-r^2/(2r_0^2)]$, where $n_{e0} = 4 \times 10^{20}\,cm^{-3}$ is the peak density and $r_0 = 1\,\mu m$ is the rms radius of the sphere. The counter-propagating laser pulse is linearly polarized in the y direction and propagates in the $-x$ direction. It has a Gaussian distribution in both transverse and longitudinal directions with $I = I_0 \cdot [w_0/w(x)]^2\exp[-2\rho^2/w^2(x)]\exp[-2t^2/\tau^2]$ where $I_0 = 6 \times 10^{22}\,Wcm^{-2}$ is the peak intensity, $w_0 = 5\,\mu m$ is the waist at
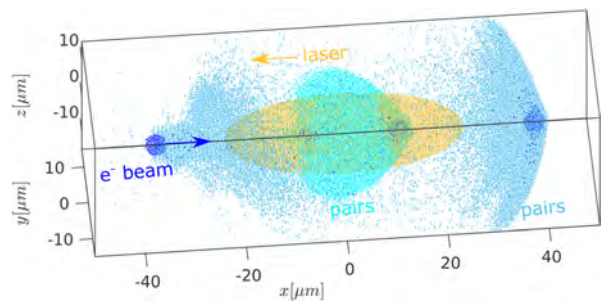

FIG. 1. Schematics of the 3D QED-PIC simulation of an energetic electron beam (deep blue) colliding with a multi-PW laser pulse (yellow) to create an electron–positron pair plasma. The volume of the pair plasma at different times is denoted as green ($t = 0.21$ ps) and light blue ($t = 0.3$ ps) dots.

$x = 0$, $w(x) = w_0\sqrt{1 + (x/x_R)^2}$, $x_R = \pi w_0^2/\lambda \approx 98\,\mu m$ is the Rayleigh length, and $\tau = 50\,\mathrm{fs}$ is the pulse duration (intensity FWHM: $\sqrt{2\log(2)}\tau \approx 59\,\mathrm{fs}$, electrical field FWHM: $2\sqrt{\log(2)}\tau \approx 83\,\mathrm{fs}$). Each dot in Fig. 1 represents a region with pair density above $2 \times 10^{20}\,\mathrm{cm}^{-3}$ or laser intensity above $5 \times 10^{20}\,\mathrm{W cm}^{-2}$. The simulation starts at $t = -0.205\,\mathrm{ps}$, and the center of laser pulse and electron beam arrive at their corresponding boundaries at $t \simeq 0$. The simulation terminates at $t = 0.32\,\mathrm{ps}$ when the laser pulse exits the simulation box.

We choose a linearly polarized laser for the simulation because it can achieve a larger pair multiplication factor compared to using a circularly polarized laser at the same energy. The higher pair multiplication origins from the exponential dependence of the pair growth rate on the field amplitude. A linearly polarized laser has $\sqrt{2}$-fold higher peak field amplitude than a circularly polarized laser at the same laser energy. When averaging over the laser period, the higher peak amplitude leads to a larger number of created pairs.

The simulations were performed using the PIC code EPOCH[101,102] with the QED module.[11,68,74] The simulation box measured $100 \times 30 \times 30\,\mu m^3$ is discretized into $4000 \times 300 \times 300$ cells. The charged particles are represented by nearly 6×10^8 computing particles. The time step is determined by both the Courant–Friedrichs–Lewy condition and the inverse plasma frequency, i.e., it is chosen as the smaller value of the minimum plasma oscillation period in any cells and the smallest cell dimension multiplied by $0.95/c$. The actual time step in our simulations is $0.083\,\mathrm{fs}$, which is well below the maximum possible photon emission time[102] $t_f \gtrsim 0.36\,\mathrm{fs}$ in all our simulations.

With the large quantum parameter, the collision quickly creates a pair plasma with an increasing charge number. Figure 2(a) shows the evolution of total charge of the injected electrons (red circles) and created electrons (blue crosses). The injected electron beam remains 1 nC throughout the interaction. The pair electron charge grows exponentially until reaching 139 nC total charge at $\sim 0.2\,\mathrm{ps}$ and then remains unchanged afterward.

The peak density of the created pairs, shown as the blue curve with cross markers in Fig. 2(b), quickly grows to a peak value of $n_p = 82n_{e0} = 3.28 \times 10^{22}\,\mathrm{cm}^{-3}$, but begins to slowly decrease at $0.17\,\mathrm{ps}$. The decrease in peak density is caused by plasma volume expansion, illustrated at three different stages in Fig. 1. The red curve in Fig. 2(b) shows the parameter n_p/γ, which determines the plasma frequency, which we will explain in detail in Sec. V. Since the pair particles are mostly created in the region of strong laser field, the pair particles immediately accelerate transversely causing volume expansion. The transverse motion, shown as the growing transverse momentum in Fig. 2(c), also allows the particle to escape the high intensity laser focus resulting in a lower total charge than predicted by Eq. (1). The blue curve with cross markers in Fig. 2(c) shows the change in pair moving direction in the later stage of cascade, and we will explain it in detail in Sec. V.

To get more insight into the dynamics of pair generation, we analyze the pair density and momentum on the centerline $y = z = 0$ with peak laser intensity. Each data point on the line is plotted as a dot in Figs. 3 and 4. The variances of the pair density and energy in the plots are caused by the stochastic nature of the QED process. The top row of these two figures shows the snapshot at $0.16\,\mathrm{ps}$. At this time, the center of the electron sphere has not reached the laser focal plane
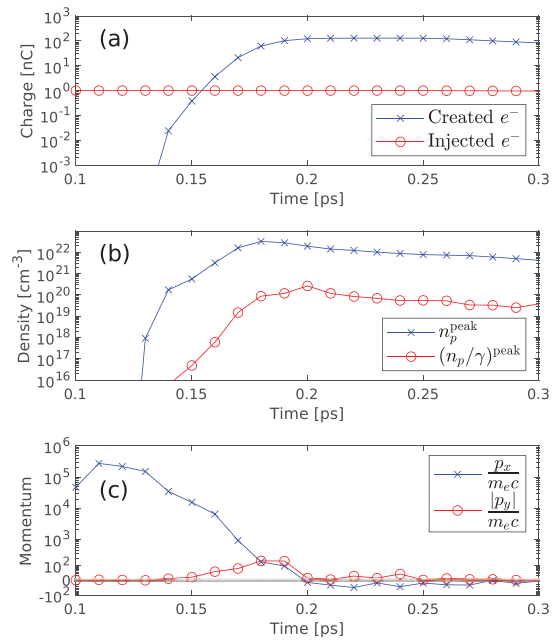

FIG. 2. (a) Evolution of total charges of the injected electrons (red) and created electrons (blue). (b) Evolution of the peak pair plasma density n_p (blue), and the parameter n_p/γ (red), which determines the laser frequency upshift. (c) Evolution of the pair particle momenta in the longitudinal (blue) and transverse (red) directions, normalized to $m_e c$. The local particle density n_p, Lorentz factor γ, and momentum $p_{x,y}$ are denoted by their respective averaged values in a single simulation cell.

though a significant amount of pairs have already been generated. The density plot in Fig. 3(a) shows that the generated pairs are limited to the region near the electron beam. The Lorentz factor plot in Fig. 3(b) shows that the electron beam energy is decreased by 2–3 orders of magnitude from its initial value $\gamma_0 = 6 \times 10^5$ after passing through the laser peak. The generated pairs have an energy of near $10^3 m_e c^2$, corresponding a quantum parameter of $\chi_e \lesssim 1$, after passing through the laser peak. This is the lowest particle energy that can be efficiently generated via the photon decay process. Beyond this point, the gamma photons can no longer decay into pairs and the QED cascade terminates, which can be seen from the saturation of charge growth in Fig. 2(a). However, the pairs continue to lose energy as shown in the last two rows of Figs. 3 and 4. We will discuss them in detail in Sec. V.

V. PAIR DECELERATION AND PAIR REFLECTION

We observed and explained in Sec. IV that the injected electron beam would emit high energy photons, which decay into pair particles in a strong laser field until the photon energy (and hence the generated pair energy) decreases to $\chi_\gamma \lesssim 1$ when the QED cascade terminates. The pairs, however, continue to lose energy via synchrotron radiation, as shown in Fig. 2(c).

The photon emission is dominated by quantum synchrotron radiation when $\chi_e \gtrsim 0.1$. The decrease in pair energy can be seen in Figs. 3(d) and 3(f), which show the snapshot immediately after the
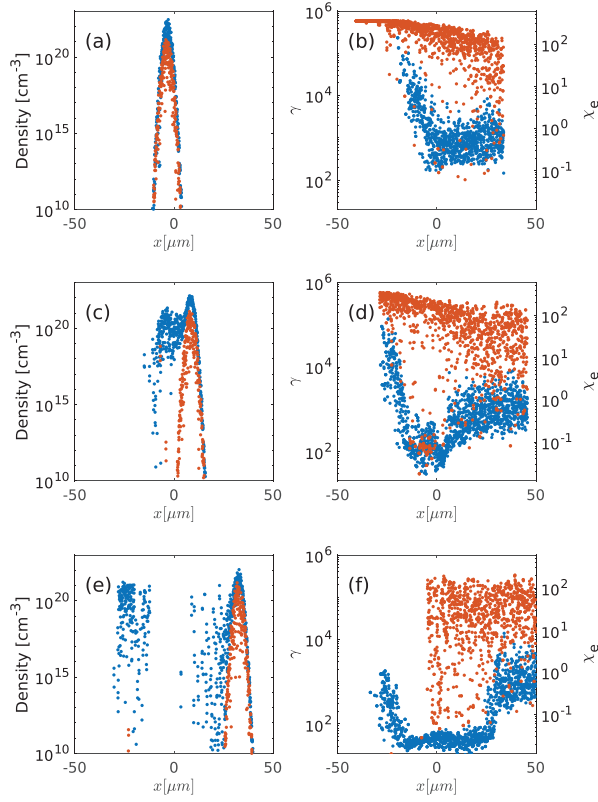
FIG. 3. The density (left column) and Lorentz factor γ (right column) of the injected electrons (red) and created electrons (blue) at line $y = z = 0$. The electron quantum factor χ_e is calculated at the peak laser amplitude $a_0 = 170$. The three rows show the snapshots at 0.16 ps (a) and (b), 0.2 ps (c) and (d), and 0.28 ps (e) and (f), respectively.

FIG. 4. The transverse p_y (left column) and longitudinal p_x (right column) momenta of the created electrons at line $y = z = 0$, normalized $m_e c$. The three rows show the snapshots at 0.16 ps (a) and (b), 0.2 ps (c) and (d), and 0.28 ps (e) and (f), respectively.

center of the electron sphere passes through the laser peak. The blue curve in Fig. 3(d) shows that the generated pair energy further decreases to $10^2 \, m_e c^2$, corresponding to $\chi_e \sim 0.1$, at the tail of the electron beam. Depending on the laser amplitude a_0, quantum synchrotron emission can reduce the pair Lorentz factor to

$$\gamma \lesssim 0.1 \frac{\gamma_0}{\tilde{\chi}_e} \approx \frac{0.05}{a_0} \frac{m_e c^2}{\hbar \omega_0}. \quad (2)$$

Figure 3(c) shows that these low-energy pairs are created through the secondary generation from the daughter pairs, and therefore, they tailgate the injected electron beam.

Quantum synchrotron emission stops when the particles lose sufficient energy or the laser amplitude becomes low, i.e., $\chi_e \lesssim 0.1$. Then, classical radiation emission begins to dominate.[2] The pair particles wiggle in the laser field to radiate electromagnetically with negligible quantum contributions like recoil or spin. The strong laser field drives transverse motion of the pairs, evidenced in Figs. 4(a) and 4(c) which show that the transverse pair momentum p_y is enveloped by the laser profile and that $|p_y|/(m_e c) = a_0$ locally. Due to the conservation of
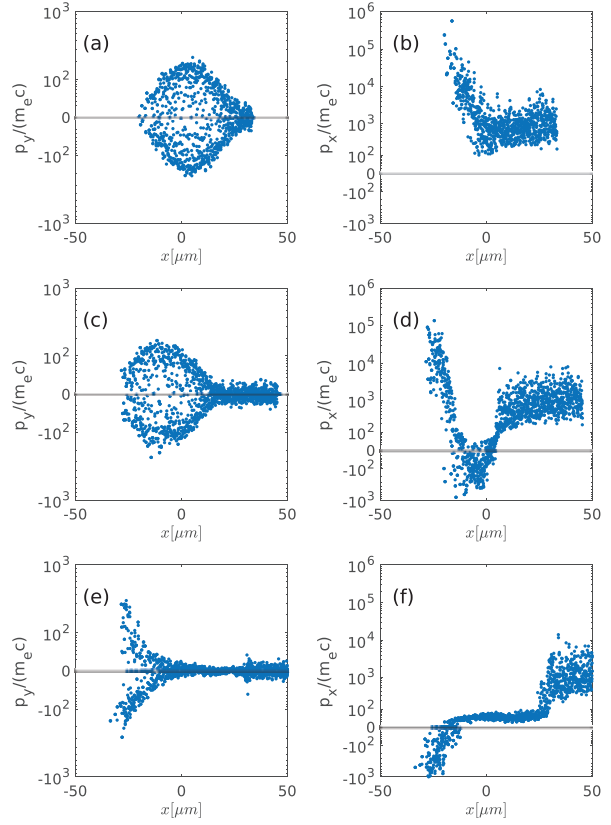
canonical momentum, each charged particle transfers an amount of $a_0^2 m_e c / (4\gamma)$ longitudinal momentum to the counter-propagating laser field upon entering it. It means that particles can be stopped or even reflected by the strong laser field if they have sufficiently low longitudinal momentum, i.e., $p_x \lesssim a_0^2 m_e c / (4\gamma)$, or equivalently, $\gamma \sim a_0$.[103] By comparing this condition with (2), we find the threshold for particle reflection

$$a_{0,\text{th}} \gtrsim \sqrt{0.05 m_e c^2 / (\hbar \omega_0)}. \quad (3)$$

For optical lasers with $\hbar \omega_0 \sim 1 \, \text{eV}$, the threshold is approximately $a_{0,\text{th}} \gtrsim 100$, corresponding to intensity $I_{\text{th}} \gtrsim 10^{22} - 10^{23} \, \text{Wcm}^{-2}$. Particle reflection is shown in Figs. 2(c), 4(d), and 4(f) as the pair longitudinal momentum p_x becomes negative near the laser peak. The reflected pair can also be observed in Fig. 1(c) in which the pairs (light blue dots) spread throughout the simulation box at $t = 0.2 \, \text{ps}$.

The particle reflection threshold is very important for probing the collective pair effects because the pair particle mass reaches their minimum value as they stop longitudinally. Since plasma dynamics is manifested through plasma frequency ω_p, which is proportional to

$\sqrt{n_p/\gamma}$, achieving lower particle energy is equally important with achieving higher particle density. Thus, we plot the parameter n_p/γ in Fig. 2(b). The red curve with circle markers shows that the parameter n_p/γ continues to increase even after the pair density reaches its peak value $n_p = 3.28 \times 10^{22}\,\mathrm{cm^{-3}}$ at $t = 0.18\,\mathrm{ps}$. The pair momentum decreases to its minimum value at $t = 0.2\,\mathrm{ps}$ when n_p/γ reaches its peak value of $2.67 \times 10^{20}\,\mathrm{cm^{-3}}$ at $t = 0.2\,\mathrm{ps}$. Thus, the beneficial synchrotron radiation, which keeps reducing the pair energy, outweighs the density decrease between $t = 0.18\,\mathrm{ps}$ and $t = 0.2\,\mathrm{ps}$ until finally the latter process dominates.

While the strong laser field causes the pairs to lose longitudinal momentum p_x, it at the same time increases the transverse momentum p_y. The maximum value of p_y is identical to local laser amplitude a_0 due to conservation of canonical momentum. Therefore, the minimum pair Lorentz factor is equal to the laser amplitude $\gamma = a_0$ provided that the particle reflection threshold condition Eq. (3) is satisfied. This is evident in Figs. 3(d) and 3(f), which show a minimum Lorentz factor of $\gamma \lesssim 100$. Note that the particle reflection may happen behind the laser peak if we consider the finite time of particle deceleration by synchrotron radiation.

Thus, the final pair density is approximately the multiplication of the quantum nonlinear parameter and the initial electron beam density; the final pair Lorentz factor is approximately equal to the laser a_0 factor, i.e.,

$$n_p \sim \tilde{\chi}_e n_e, \quad \gamma_f \sim a_0. \tag{4}$$

These relations are valid if the laser is above the threshold intensity I_{th} for particle reflection (3), and if the interaction time is long enough such that the cascade reaches its asymptotic state.

To illustrate the creation of pairs more clearly, we plot the profiles of pair density and laser intensity in the $y = 0$ plane and $z = 0$ plane as the top and bottom panels of Fig. 5, respectively. Each red dot denotes a region with $n_p/\gamma > 1 \times 10^{19}\,\mathrm{cm^{-3}}$ at the corresponding plane. It is seen in Fig. 5(a) that the pairs are initially created near the injected electron beam. They then expand in mainly transverse directions shortly after creation. Linear laser polarization breaks the cylindrical symmetry of pair motion. The y-polarized laser naturally accelerates the pairs more strongly in the y direction than in the z direction, which is seen in Fig. 5(b). The asymmetry of pair expansion increases as shown in Fig. 5(c). Figure 5(c) also reveals rich dynamics of the laser profile, which will be discussed in detail in Sec. VI.

VI. LASER BEAM DIFFRACTION AND FREQUENCY UPCONVERSION

Since the pair generation rate is proportional to laser amplitude, the pairs are dominantly created near the peak laser field. Strong laser field, thus, drives pairs into oscillation immediately after they are generated. The induced transverse current radiates electromagnetic fields. With non-negligible pair density, the radiation could reach a detectable level to reveal the pair dynamics. When pair density reaches near the critical density, the radiation becomes strongly coupled to the input laser, causing a quantitative upshift of laser frequency. Measuring the change in laser frequency allows us to unambiguously probe collective pair plasma effects.

Macroscopically, laser frequency upshift arises from non-adiabatic change of index of refraction, which determines the phase velocity of light. Suddenly created pairs reduce the index of refraction,
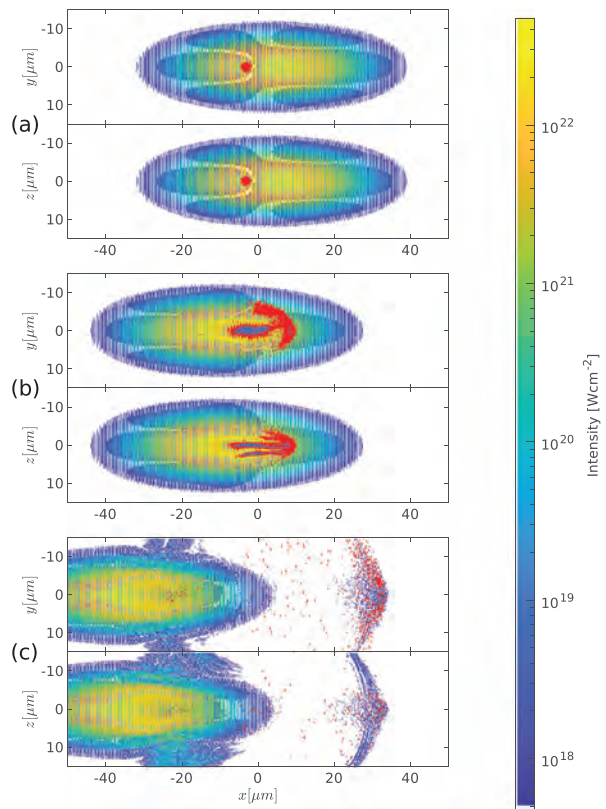

FIG. 5. The two panels of each subplot show the laser profiles at the $z = 0$ cross section and $y = 0$ cross section, respectively. The red dots show the regions of $n_p/\gamma > 1 \times 10^{19}\,\mathrm{cm^{-3}}$ at the corresponding planes. The snapshots are taken at 0.16 ps (a), 0.2 ps (b), and 0.28 ps (c), respectively.

thereby increasing the laser phase velocity. It corresponds to an increased rate of local laser phase oscillation and, thus, an upshift of the laser frequency.

Microscopically, the laser frequency upshift can be analyzed through finding the transverse current $\boldsymbol{J}_\perp$ of pair particles. As pairs are almost always generated when the strong laser field is present, they are immediately driven into an oscillatory motion. Assuming that the pair particles have no transverse momentum at the time of generation. Laser field with vector potential $\boldsymbol{A}$ can transfer transverse momentum of $\boldsymbol{p}_\perp = e\boldsymbol{A}_\perp$ to the pairs. Thus, the pair transverse current is $\boldsymbol{J}_\perp = 2en_p\boldsymbol{p}_\perp/(\gamma m_e) = (2e^2 n_p/m_e)\boldsymbol{A}_\perp/\gamma = \varepsilon_0\omega_p^2\boldsymbol{A}_\perp$ where ε_0 is the permittivity of vacuum. Here, we identified the plasma frequency $\omega_p \equiv [2n_p e^2/(\gamma m_e \varepsilon_0)]^{1/2}$. The factor of two accounts for the equal contribution of positrons and electrons to the laser dispersion relation. Transverse current couples to the laser field through the wave equation

$$\nabla^2 \boldsymbol{A}_\perp - \frac{1}{c^2}\partial_t^2 \boldsymbol{A}_\perp = \frac{e^2}{m_e c^2 \varepsilon_0}\frac{2n_p}{\gamma}\boldsymbol{A}_\perp \equiv \frac{\omega_p^2}{c^2}\boldsymbol{A}_\perp, \tag{5}$$

from which we see that a non-adiabatic change of plasma frequency $\omega_p^2 \propto n_p/\gamma$ induces a change in laser frequency ω. If the plasma frequency is small compared with the input laser frequency $\omega_p \ll \omega$, the laser frequency is approximated as

$$\omega \cong \omega_0 + \omega_p^2/(2\omega_0). \tag{6}$$

If the plasma is created non-instantly, the change in laser frequency could be expressed in an integral form of the plasma frequency change at the retarded position $X = x + c(t - t')$:

$$\omega(x,t) = \omega_0(x) + \frac{1}{2\omega_0} \int_0^t dt' \left[\partial_T \omega_p^2(X,T) \right]_{X=x+c(t-t')}^{T=t'}. \tag{7}$$

The laser wave vector changes correspondingly obeying the dispersion relation

$$k(x,t) \cong \omega(x,t)/c - \omega_p^2(x,t)/(2\omega_0 c)$$
$$= k_0(x) + \frac{1}{2\omega_0} \int_0^t dt' \left[\partial_X \omega_p^2(X,T) \right]_{X=x+c(t-t')}^{T=t'}. \tag{8}$$

Equations (7) and (8) demonstrate that the change in laser frequency and wave vector is determined by the total temporal and spatial change in plasma density, respectively. In the limit of instantaneous plasma creation, the upshift of frequency and wave vector after interaction reduce to simple forms $\Delta\omega \equiv \omega - \omega_0 = \omega_p^2/(2\omega_0)$ and $\Delta k \equiv k - k_0 = \omega_p^2/(2c\omega_0)$. The relation of instantaneous laser frequency and wave vector, $\Delta\omega = c\Delta k$, becomes very useful for interpreting our numerical simulation results: whereas experiments measure laser frequency at a specific location, numerical simulations often more conveniently output laser wave vector at a specific time. Equations (7) and (8) provide a definite relation to transform the laser wave vector upshift into frequency upshift during QED cascade.

For the simulation under consideration, the peak value of n_p/γ corresponds to 6.7% of the critical plasma density at rest $n_c \approx 1.71 \times 10^{21}$ cm^{-3} of the drive laser. Accordingly, a laser frequency upshift is observed in the intensity spectra displayed in Fig. 6. Figure 6(a) shows the laser intensity in its propagation axis $y = z = 0$ with each curve corresponding to times from $t = 0.16$ to 0.24 ps, respectively, in direction of the arrow. Figure 6(b) shows the corresponding intensity spectra by Fourier transformation. The peaks of the spectra before and after collision reveal a wave vector upshift $\Delta k/k_0 = 0.2\%$. Since the laser pulse propagates against the pair plasma, its wave vector spectrum becomes equivalent to the frequency spectrum after collision: 0.2% is also the laser frequency upshift. This finite frequency upshift is caused by the small fraction of laser overlap with the electron beam. Specifically, the frequency-upconverted photons are confined to a small region, whereas the majority of laser photons are not upconverted.

The oscillatory motion of the high density pairs absorbs a significant amount of laser energy. Combined with the QED process, it causes a decrease in laser peak intensity, which can be observed in Fig. 6. We highlight this process between $t = 0.18$ ps and 0.21 ps as thick curves in Fig. 6(a). This period corresponds to when the pair parameter n_p/γ approaches its peak value, as can be seen from Fig. 2(b). Actually, the pairs, after absorbing the laser energy, radiate to the whole space. It is revealed in Fig. 6(a) which shows splitting of the laser peak when the
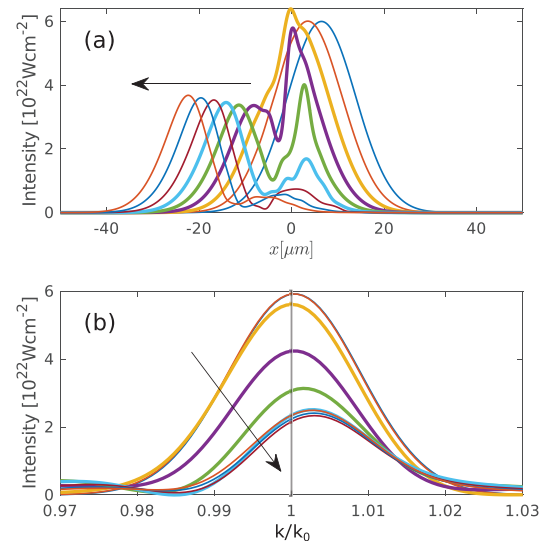

FIG. 6. (a) The laser pulse intensity envelopes between $t = 0.16$ ps and 0.24 ps with an increase in time in the direction of the arrow. (b) The laser intensity spectra at the corresponding times.

pairs are generated and laser frequency is upshifted. While the main laser peak continues to propagate to the $-x$ direction, a second peak is developed at $t = 0.19$ ps (thick purple curve) and propagates toward the $+x$ direction.

Due to the small volume of the pairs, they emit a point-source-like radiation, as shown in Fig. 5(c). The large radiation angle can actually be used advantageously for experimental detection: It can be captured by an optical detector installed away from the path of laser beam. The radiation is near optical frequency and is, hence, easily distinguished from high energy gamma photons.

Much higher laser frequency upshift can be obtained when focusing on the region where pairs are quickly created. Such a laser spectrogram is typically obtained in experiments using techniques like frequency-resolved optical gating[104] or spectral shear interferometry for direct electric field reconstruction.[105] Numerically, we conduct a wavelet transform of the laser pulse and obtain precisely the laser photon wave vectors at different pulse positions plotted as red curves in Fig. 7. We also plot the pair particle density in the $z = 0$ plane to demonstrate the correlation of pair plasma creation and laser wave vector upshift. Figure 7(a) shows that the wave vector spectrum becomes chirped immediately at the region of plasma creation near $x = 0$. The wave vector chirps up in the front of the interaction region and chirps down in the tail, which agrees with Eq. (8). As the pair density increases and the interaction continues, the amplitude of chirp grows, as seen in Fig. 7(b). The chirped region propagates along the laser direction [Fig. 7(c)] and gets separated with the pair plasma. Thus, it can eventually be collected by a detector and revealing the a chirped frequency spectrum. The maximum photon frequency shift reaches $\Delta\omega/\omega_0 = 2.4\%$.

The small disturbance in laser phase and intensity can be precisely measured with an interferometer. As shown in Fig. 8, the strong
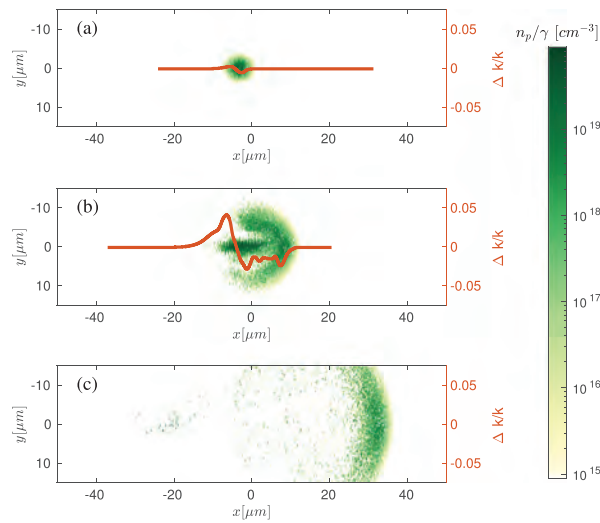
FIG. 7. The pair parameter n_p/γ and the relative laser wave number change $\Delta k/k$. The snapshots are taken at 0.16 ps (a), 0.2 ps (b), and 0.28 ps (c), respectively.

laser is first sent through a beam splitter with a large reflection ratio. A small fraction of the laser pulse is split to serve as a reference beam, whose electric field can be denoted as $E_r = E_{r0}(\mathbf{r},t)e^{-i\omega_0 t} + c.c.$ The strong laser pulse, after interacting with the electron beam, becomes $E = E_0(\mathbf{r},t)e^{-i\omega_0 t+i\varphi} + c.c.$. Here, $\varphi \equiv \int_0^t \Delta\omega dt'$ represents the accumulated local phase change and $E_0(\mathbf{r},t)$ denotes the new envelope. The pulse is then attenuated to the same amplitude with the reference beam before they are combined through another beam splitter. The interference signal, called a homodyne signal, is

$$\Delta I = \frac{1}{T}\int_0^T \frac{c\varepsilon_0}{2}|E_r - E|^2 dt, \tag{9}$$

where the negative sign arises from the double reflection of the PW laser and the signal is averaged through an optical cycle $T = 2\pi/\omega_0$ to model the slow response time of the photo detector. The homodyne signal is sensitive to both the laser phase fluctuation and envelope change. For only a small phase fluctuation $\varphi \ll 2\pi$, the homodyne signal is proportional to the accumulated phase φ, i.e.,
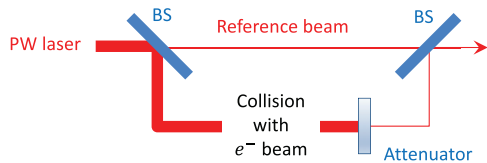

FIG. 8. Interferometer setup for homodyne detection of the change in laser profile. A weak reference beam is split from the strong PW laser using a beam splitter (BS) with a large reflection ratio. The same reference beam is then combined with the attenuated post-interaction PW laser to produce the interference signal.

$$\Delta I \propto [1 - \cos(\varphi)]I_{r0} \approx \varphi I_{r0}, \tag{10}$$

where I_{r0} is the intensity of the reference beam. Since $\varphi = \int_0^t \Delta\omega dt'$, one can find out the frequency shift $\Delta\omega$ through $\Delta I/I_{r0}$. Note that the proportional relation in Eq. (10) only holds for $\Delta I \ll I_{r0}$.

Numerically, we show the homodyne signal $(c\varepsilon_0/2)|E_r - E|^2$ at three different snapshots in Fig. 9 assuming instantaneous detector response time. Slower detectors will not detect the wavelength-scale fringes, but the intensity envelope will be the same. The reference beam is obtained via a separate simulation of the same laser beam without encountering the electron beam. The interference signifies the change in an electromagnetic field. The radiation pattern in Fig. 9(c) consists of two types of signals, including a pattern that propagates along the laser direction and a pattern that radiates to the whole space. The propagation radiation pattern is the result of interference of phase-shifted post-interaction beam and the reference beam. The latter radiation pattern is the point-source-like pair emission caused by the finite pair plasma size. It confirms that the radiation starts at the location where pairs are generated and then expands to the whole space.

VII. SCALING OF THE LASER FREQUENCY UPSHFIT

Since upconversion of laser frequency is determined by the pair plasma frequency, it provides an unambiguous signature of collective plasma effects in beam-driven QED cascades. In Sec. VI, our 3D PIC simulations demonstrate the collective pair plasma effects during pair creation and energy decay and show how the plasma signature is imprinted in the colliding laser. For purposes of illustration, the collision uses a 24 PW laser pulse and a 1 nC electron beam at 300 GeV. However, can existing technology produce sufficiently high density pair plasma to exhibit observable collective effects? In this section, we answer the question by finding how the amount of frequency upshift scales with different parameters of the laser and electron beam.
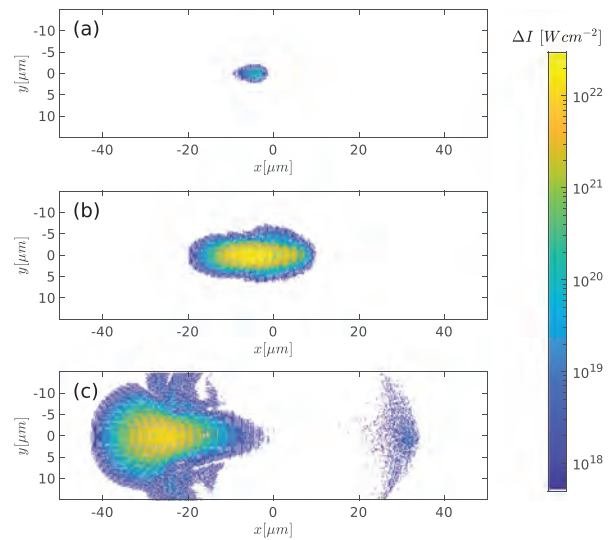

FIG. 9. The homodyne signal, which shows the change in laser beam intensity profile at the $z = 0$ cross section. The snapshots are taken at 0.16 ps (a), 0.2 ps (b), and 0.28 ps (c), respectively.

It is made clear in Eqs. (5) and (6) that the magnitude of pair plasma radiation is determined by the pair plasma parameter n_p/γ, i.e., plasma density divided by pair energy. The spatial profile of the radiation depends on the pair size at the time of pair creation. High pair density is achieved through high input electron beam density n_e and large pair multiplication factor $\tilde{\chi}$, which, according to Eq. (1), are proportional to the laser amplitude a_0, laser frequency ω_0, and electron beam energy $\gamma_0 m_e c^2$.

For exhibiting collective effects, an equally important parameter is the pair energy or Lorentz factor. In a QED cascade, the pair energy decreases as a result of radiation recoil and the ponderomotive potential of laser field, as we explained in Sec. IV. The minimum pair energy is reached when the laser intensity meets the threshold for pair reflection, as shown in Eq. (3). Then, the pair motion becomes purely transverse and the pair Lorentz factor. reduces to a_0, as shown in Eq. (4). By combining Eqs. (6) and (4), we find the frequency upshift

$$\omega_f^2/\omega_0^2 - 1 \sim \frac{\tilde{\chi}_e n_e}{n_c a_0} \sim \gamma_0 \frac{\hbar\omega_0}{m_e c^2} \frac{n_e}{n_c}. \tag{11}$$

This relation holds if the laser pulse is sufficiently long and intense such that the QED cascade fully develops and the pair plasma is eventually stopped and reflected.

The scaling relation [Eq. (11)] is verified through a series of 1D QED-PIC simulations as reported in Ref. 75. The data show that increasing either beam density or beam energy causes a linear increase in the created pair plasma density, whereas the final pair Lorentz factor remains constant at about a_0. They both results in a linear increase in the maximum frequency upshift.

The effect of higher laser intensity has a threshold dependence. When the laser intensity is below 3×10^{22} Wcm^{-2}, the pair reflection condition (3) is not satisfied and the cascade does not saturate within the pulse duration, causing minimum laser frequency upshift. However, above the threshold amplitude, the quantity n_p/γ becomes independent of the laser intensity and the laser frequency upshift reaches its maximum value.

VIII. COLLISION OF 3 PW LASER AND 30 GEV ELECTRON BEAM

In Secs. IV–VII we presented a clear numerical demonstration that the interplay between collective plasma and strong-field quantum effects leaves a characteristic imprint on the driving laser pulse. The upshift of the instantaneous laser frequency, according to the "rule of thumb" (11), becomes experimentally observable by combining a multi-GeV class electron beam with density above $\sim 10^{20}$ cm^{-3} and a laser at $\sim 10^{22}$ Wcm^{-2} intensity. In principle, such beam-driven QED cascades could be initiated with electron beams obtained from either a linear accelerator or laser wakefield acceleration (LWFA) at all-optical laser facilities. However, linear accelerators benefit from their much higher nC-level total charge number compared with the pC-level obtained from the reported LWFA accelerated electrons.[106] The required electron beam density and beam energy can be obtained with only a moderate upgrade of existing facilities, e.g., SLAC's FACET-II.[79]

We conduct such 3D QED-PIC simulations to show this prospect. Figure 10 illustrates the simulation of a 50 fs-duration, 2.5 μm-waist, 3 PW (3×10^{22} Wcm^{-2}) laser pulse[78] colliding with a 1 nC, 30 GeV, 4×10^{20} cm^{-3} electron beam.[79] Other numerical parameters
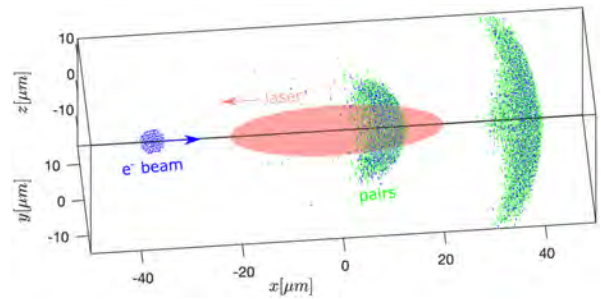

FIG. 10. 3D simulation of a 30 GeV (blue) electron beam colliding with a 3 PW laser pulse (red). A QED cascade creates a pair plasma (green) with an expanding volume. The electron beam itself also expands due to the laser ponderomotive force.

are identical to the last 3D simulations. The generated pair plasma and the radiation are shown in Figs. 11 and 12. Figures 11(a) and 11(b) show that the created electron–positron pair plasma reaches a total charge number of 26 nC and peak density of 6.8×10^{21} cm^{-3}. The red dots in Fig. 12 show that the tightly focused laser punches a hole in the pair plasma and pushes the pairs away from the propagation axis.
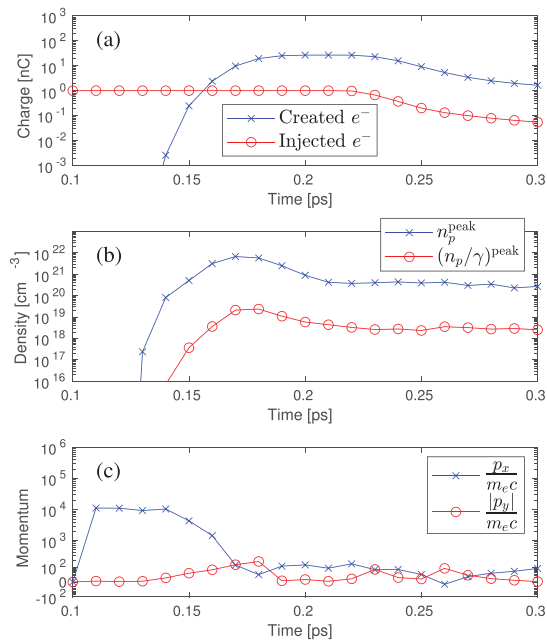

FIG. 11. (a) Evolution of total charges of the injected 30 GeV electrons (red) and the created electrons (blue). (b) Evolution of the peak pair plasma density n_p (blue) and the parameter n_p/γ (red), which determines the laser frequency upshift. (c) Evolution of the pair particle momenta in the longitudinal (blue) and transverse (red) directions, normalized to $m_e c$. The local particle density n_p, Lorentz factor γ, and momentum $p_{x,y}$ denote their respective averaged values in a single simulation cell.
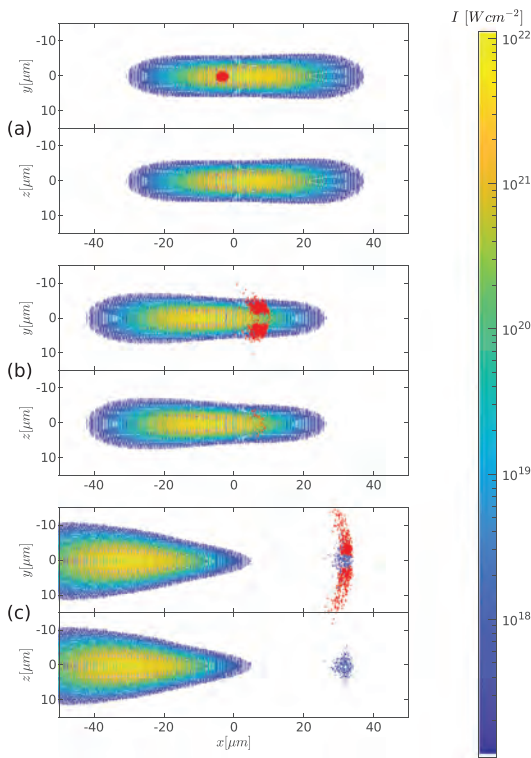
FIG. 12. The two panels of each subplot show the laser profiles at the $z = 0$ cross section and $y = 0$ cross section, respectively. The red dots show the regions of $n_p/\gamma > 1 \times 10^{19}$ cm^{-3} at the corresponding planes. The snapshots are taken at 0.16 ps (a), 0.18 ps (b), and 0.24 ps (c), respectively.

The created pairs begin to escape the simulation box from $t = 0.23$ ps causing a decrease in total charge number as seen in Fig. 11(a).

With a lower energy, the injected electron beam has a much lower relativistic mass. The electrons are, thus, expelled by the strong laser ponderomotive force, and they expand with the created pair plasma. This is seen in Fig. 10 where the blue dots mostly overlap with the green shades whereas the blue dots remain a sphere shape in Fig. 1. The expanding electron beam begins to leave the simulation box, causing a decreasing total charge from $t = 0.23$ ps as seen in Fig. 11(a).

Since the laser intensity meets the threshold value $a_{0,\text{th}}$ for particle reflection, some pairs reverse their propagation direction. This is confirmed in Fig. 11(c) as the pair longitudinal momentum changes sign. The parameter n_p/γ reaches 2.4×10^{19} cm^{-3}, corresponding to 1.4% of the critical density of a 0.8 μm laser.

We obtain the instantaneous wave vectors through a wavelet transform of the laser electric field at $y = z = 0$ and plot them as red curves in Fig. 13. For comparison, we also plot the wave vectors of the same laser without encountering an electron beam as black curves. Due to the tight focus, the laser has a short Rayleigh length, so the Gouy phase induces a down chirp of the wave vectors near the focal point. The red curves clearly show a laser wave vector upshift in the
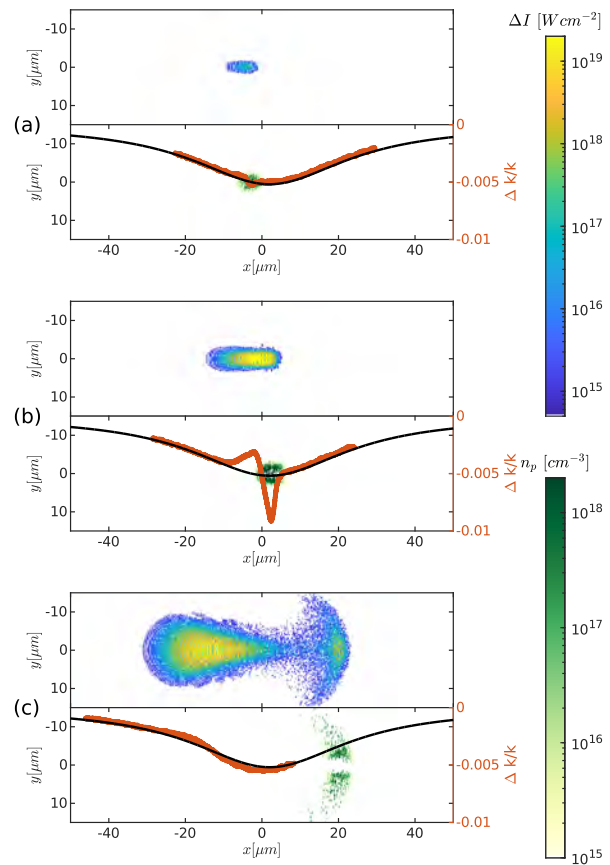

FIG. 13. The top panel of each subplot shows the homodyne signal at the $z = 0$ cross section. The bottom panel shows the pair parameter n_p/γ at the $z = 0$ cross section. The red and black curves show the instantaneous wave vectors of the laser field at $y = z = 0$ with and without encountering the electron beam, respectively. The snapshots are taken at 0.16 ps (a), 0.18 ps (b), and 0.24 ps (c), respectively.

region of pair plasma creation. The maximum wave vector upshift reaches a value of $\sim$0.2%. The value, however, decreases as the pair plasma expands.

In the top panels of Fig. 13, we plot the homodyne signal $(c\varepsilon_0/2)|E - E_r|$. Strong signals are exhibited in the regions of pair plasma creation. The plots show that the interference signal immediately appears when the pairs are initially created. As the pair density grows, the signal reaches a maximum intensity of 1.2×10^{20} Wcm^{-2}, which can be easily detected in an experiment. At $t \geq 0.18$ ps, the homodyne signal intensity increases by 5×10^{19} Wcm^{-2} within a single laser period indicating a 0.16% laser wave vector upshift.

IX. SUMMARY AND DISCUSSION

In couching the demonstration of collective plasma effects in the QED plasma regime as a joint production-observation problem, we showed, using PIC simulations, how collective effects may in fact be

both produced and observed in high-density electron–positron pair plasmas through strong-field QED cascades using existing laser and electron beam technologies. Both high pair density n_p and low pair Lorentz factor γ are shown to be equally important for exhibiting the strong collective plasma effects. A large pair plasma frequency can be achieved with a dense and high-energy electron beam. A higher laser intensities, however, does not always benefit laser frequency upshift. A higher laser intensity can effectively increase the pair plasma frequency only below the threshold amplitude $a_{0,th} \gtrsim 100$ ($I_{0,th} \gtrsim 10^{22}$ Wcm^{-2}). With pairs being stopped, higher laser intensities above the threshold drive larger transverse momentum and, thus, suppress the growth of plasma frequency.

We specifically considered two sets of 3D PIC simulations, including one set with ideal parameters and the other set with existing technologies. The ideal parameter set uses a 24PW $\lambda = 0.8\,\mu$m laser with a waist of 5 μm, a duration of 50 fs, and a peak intensity of 6×10^{22} Wcm^{-2} (corresponding to $a_0 \approx 170$). Combined with a 300 GeV, 1nC, 4×10^{20} cm^{-3} peak density electron beam, it creates a 139nC plasma with the peak density of 3.28×10^{22} cm^{-3}, which is 82 times higher than the injected electron beam. The pair parameter n_p/γ reaches a peak value of 2.67×10^{20} cm^{-3}, which is 6.7% of the critical density of the laser. The simulation shows a laser frequency upshift of 2.4% at the output and a maximum wave vector upshift of 4.8% during the collision.

We further demonstrated that the collective QED plasma signature can be observed with state-of-the-art technologies. Even a 30 GeV electron beam and a 3PW 2.5 μm-waist laser (other parameters are identical to the previous 3D PIC simulation) can create a pair plasma of $n_p/\gamma = 2.67 \times 10^{20}$ cm^{-3} and induce a 0.2% laser frequency upshift. It suggests how hitherto unobserved collective effects can be probed with existing state-of-the-art laser and beam technologies, offering a strong argument for collocating these technologies.

What emerges from these simulations is a picture of how the co-location[107,108] of a dense, 30 GeV electron beam with a 3–10 PW optical laser enables us to reach the QED plasma regime at substantially lower laser intensities (10^{22} Wcm^{-2}) than previously thought possible. Whereas it has been well known that QED cascades can be studied in electron beam laser collisions,[3] our simulations highlight the importance of the electron beam density, showing that the beam-compression techniques developed in the context of FACET-II are indeed sufficient to describe the interplay between collective plasma and strong-field quantum effects with a laser–electron beam setup. In fact, compared to all-optical methods of reaching the QED regime, the use of lower laser intensities reduces the particle mass shift, thereby remarkably making the QED collective effects easier to observe.

It can be imagined that further, possibly more distinct, signatures of the collective effects recognized here might be obtained through variations of the laser or the beam parameters envisioned here. However, what is clear is that the beam-laser collision setup, together with the methodology of witnessing collective effects through laser frequency shifts, as envisioned here, already opens up possibilities for the near-term studying of the QED plasma regime with presently available technology.

ACKNOWLEDGMENTS

AUTHOR DECLARATIONS
Conflict of Interest

The authors have no conflicts to disclose.

DATA AVAILABILITY

The data that support the findings of this study are available from the corresponding author upon reasonable request.

REFERENCES

[1] J. Schwinger, "On gauge invariance and vacuum polarization," Phys. Rev. **82**, 664 (1951).

[2] A. Di Piazza, C. Müller, K. Z. Hatsagortsyan, and C. H. Keitel, "Extremely high-intensity laser interactions with fundamental quantum systems," Rev. Mod. Phys. **84**, 1177 (2012).

[3] I. V. Sokolov, N. M. Naumova, J. A. Nees, and G. A. Mourou, "Pair creation in QED-strong pulsed laser fields interacting with electron beams," Phys. Rev. Lett. **105**, 195005 (2010).

[4] H. Hu, C. Müller, and C. H. Keitel, "Complete QED theory of multiphoton trident pair production in strong laser fields," Phys. Rev. Lett. **105**, 080401 (2010).

[5] A. G. R. Thomas, C. P. Ridgers, S. S. Bulanov, B. J. Griffin, and S. P. D. Mangles, "Strong radiation-damping effects in a gamma-ray source generated by the interaction of a high-intensity laser with a wakefield-accelerated electron beam," Phys. Rev. X **2**, 041004 (2012).

[6] N. Neitz and A. Di Piazza, "Stochasticity effects in quantum radiation reaction," Phys. Rev. Lett. **111**, 054802 (2013).

[7] S. S. Bulanov, C. B. Schroeder, E. Esarey, and W. P. Leemans, "Electromagnetic cascade in high-energy electron, positron, and photon interactions with intense laser pulses," Phys. Rev. A **87**, 062110 (2013).

[8] T. G. Blackburn, C. P. Ridgers, J. G. Kirk, and A. R. Bell, "Quantum radiation reaction in laser–electron-beam collisions," Phys. Rev. Lett. **112**, 015001 (2014).

[9] D. G. Green and C. N. Harvey, "Transverse spreading of electrons in high-intensity laser fields," Phys. Rev. Lett. **112**, 164801 (2014).

[10] M. Vranic, J. L. Martins, J. Vieira, R. A. Fonseca, and L. O. Silva, "All-optical radiation reaction at 10^{21} Wcm^2," Phys. Rev. Lett. **113**, 134801 (2014).

[11] T. G. Blackburn, A. Ilderton, C. D. Murphy, and M. Marklund, "Scaling laws for positron production in laser–electron-beam collisions," Phys. Rev. A **96**, 022128 (2017).

[12] M. Vranic, O. Klimo, G. Korn, and S. Weber, "Multi-GeV electron–positron beam generation from laser–electron scattering," Sci. Rep. **8**, 4702 (2018).

[13] J. Magnusson, A. Gonoskov, M. Marklund, T. Z. Esirkepov, J. K. Koga, K. Kondo, M. Kando, S. V. Bulanov, G. Korn, and S. S. Bulanov, "Laser-particle collider for multi-GeV photon production," Phys. Rev. Lett. **122**, 254801 (2019).

[14] V. M. Kaspi and A. M. Beloborodov, "Magnetars," Annu. Rev. Astron. Astrophys. **55**, 261 (2017).

[15] B. Cerutti and A. M. Beloborodov, "Electrodynamics of pulsar magnetospheres," Space Sci. Rev. **207**, 111 (2017).

[16] Y. Q. Xue, X. C. Zheng, Y. Li, W. N. Brandt, B. Zhang, B. Luo, B. B. Zhang, F. E. Bauer, H. Sun, B. D. Lehmer, X. F. Wu, G. Yang, X. Kong, J. Y. Li, M. Y. Sun, J. X. Wang, and F. Vito, "A magnetar-powered x-ray transient as the aftermath of a binary neutron-star merger," Nature **568**, 198 (2019).

[17] D. J. Price and S. Rosswog, "Producing ultrastrong magnetic fields in neutron star mergers," Science **312**, 719 (2006).

[18] P. Mösta, C. D. Ott, D. Radice, L. F. Roberts, E. Schnetter, and R. Haas, "A large-scale dynamo and magnetoturbulence in rapidly rotating core-collapse supernovae," Nature **528**, 376 (2015).

[19] S. Akiyama, J. C. Wheeler, D. L. Meier, and I. Lichtenstadt, "The magnetorotational instability in core-collapse supernova explosions," Astrophys. J. **584**, 954 (2003).

[20] L. Lin, C. F. Zhang, P. Wang, H. Gao, X. Guan, J. L. Han, J. C. Jiang, P. Jiang, K. J. Lee, D. Li, Y. P. Men *et al.*, "No pulsed radio emission during a bursting phase of a Galactic magnetar," Nature **587**, 63 (2020).

[21]A. Ridnaia, D. Svinkin, D. Frederiks, A. Bykov, S. Popov, R. Aptekar, S. Golenetskii, A. Lysenko, A. Tsvetkova, M. Ulanov, and T. L. Cline, "A peculiar hard x-ray counterpart of a galactic fast radio burst," Nat. Astron. **5**, 372 (2021).

[22]C. K. Li, L. Lin, S. L. Xiong, M. Y. Ge, X. B. Li, T. P. Li, F. J. Lu, S. N. Zhang, Y. L. Tuo, Y. Nang et al., "HXMT identification of a non-thermal x-ray burst from SGR J1935 + 2154 and with FRB 200428," Nat. Astron. **5**, 378 (2021).

[23]C. D. Bochenek, V. Ravi, K. V. Belov, G. Hallinan, J. Kocz, S. R. Kulkarni, and D. L. McKenna, "A fast radio burst associated with a Galactic magnetar," Nature **587**, 59 (2020).

[24]The CHIME/FRB Collaboration, "A bright millisecond-duration radio burst from a Galactic magnetar," Nature **587**, 54 (2020).

[25]A. Y. Chen, F. Cruz, and A. Spitkovsky, "Filling the magnetospheres of weak pulsars," Astrophys. J. **889**, 69 (2020).

[26]A. N. Timokhin and A. K. Harding, "On the maximum pair multiplicity of pulsar cascades," Astrophys. J **871**, 12 (2019).

[27]R. Gueroult, Y. Shi, J.-M. Rax, and N. J. Fisch, "Determining the rotation direction in pulsars," Nat. Commun. **10**, 3232 (2019).

[28]D. B. Melrose and R. Yuen, "Pulsar electrodynamics: An unsolved problem," J. Plasma Phys. **82**, 635820202 (2016).

[29]B. Marcote, K. Nimmo, J. W. T. Hessels, S. P. Tendulkar, C. G. Bassa, Z. Paragi, A. Keimpema, M. Bhardwaj, R. Karuppusamy, V. M. Kaspi et al., "A repeating fast radio burst source localized to a nearby spiral galaxy," Nature **577**, 190 (2020).

[30]The CHIME/FRB Collaboration, "A second source of repeating fast radio bursts," Nature **566**, 235 (2019).

[31]V. Ravi, M. Catha, L. D'Addario, S. G. Djorgovski, G. Hallinan, R. Hobbs, J. Kocz, S. R. Kulkarni, J. Shi, H. K. Vedantham, S. Weinreb, and D. P. Woody, "A fast radio burst localized to a massive galaxy," Nature **572**, 352 (2019).

[32]K. W. Bannister, A. T. Deller, C. Phillips, J.-P. Macquart, J. X. Prochaska, N. Tejos, S. D. Ryder, E. M. Sadler, R. M. Shannon, S. Simha et al., "A single fast radio burst localized to a massive galaxy at cosmological distance," Science **365**, 565 (2019).

[33]D. A. Uzdensky and S. Rightley, "Plasma physics of extreme astrophysical environments," Rep. Prog. Phys. **77**, 036902 (2014).

[34]D. Uzdensky, M. Begelman, A. Beloborodov, R. Blandford, S. Boldyrev, B. Cerutti, F. Fiuza, D. Giannios, T. Grismayer, M. Kunz, N. Loureiro, M. Lyutikov, M. Medvedev, M. Petropoulou, A. Philippov, E. Quataert, A. Schekochihin, K. Schoeffler, L. Silva, L. Sironi, A. Spitkovsky, G. Werner, V. Zhdankin, J. Zrake, and E. Zweibel, "Extreme plasma astrophysics," arXiv:1903.05328 (2019).

[35]P. Zhang, S. S. Bulanov, D. Seipt, A. V. Arefiev, and A. G. R. Thomas, "Relativistic plasma physics in supercritical fields," Phys. Plasmas **27**, 050601 (2020).

[36]M.-H. Wang, S.-K. Ai, Z.-X. Li, N. Xing, H. Gao, and B. Zhang, "Testing the hypothesis of a compact-binary-coalescence origin of fast radio bursts using a multimessenger approach," Astrophys. J. **891**, L39 (2020).

[37]B. P. Abbott, R. Abbott, T. D. Abbott, S. Abraham, F. Acernese, K. Ackley, C. Adams, R. X. Adhikari, V. B. Adya, C. Affeldt et al., "GW190425: Observation of a compact binary coalescence with total mass ∼3.4 M⊙," Astrophys. J. **892**, L3 (2020).

[38]LIGO Scientific Collaboration and Virgo Collaboration, "GW170817: Observation of gravitational waves from a binary neutron star inspiral," Phys. Rev. Lett. **119**, 161101 (2017).

[39]C. Palenzuela, L. Lehner, M. Ponce, S. L. Liebling, M. Anderson, D. Neilsen, and P. Motl, "Electromagnetic and gravitational outputs from binary-neutron-star coalescence," Phys. Rev. Lett. **111**, 061105 (2013).

[40]M. Anderson, E. W. Hirschmann, L. Lehner, S. L. Liebling, P. M. Motl, D. Neilsen, C. Palenzuela, and J. E. Tohline, "Magnetized neutron-star mergers and gravitational-wave signals," Phys. Rev. Lett. **100**, 191101 (2008).

[41]Ó. Amaro and M. Vranic, "Optimal laser focusing for positron production in laser–electron scattering," New J. Phys. **23**, 115001 (2021).

[42]W. Luo, W.-Y. Liu, T. Yuan, M. Chen, J.-Y. Yu, F.-Y. Li, D. Del Sorbo, C. P. Ridgers, and Z.-M. Sheng, "QED cascade saturation in extreme high fields," Sci. Rep. **8**, 8400 (2018).

[43]J.-X. Liu, Y. Zhao, X.-P. Wang, J.-Z. Quan, T.-P. Yu, G.-B. Zhang, X.-H. Yang, Y.-Y. Ma, F.-Q. Shao, and J. Zhao, "High-flux positrons generation via

two counter-propagating laser pulses irradiating near-critical-density plasmas," Phys. Plasmas **25**, 103106 (2018).

[44]Z. Guo, L. Ji, Q. Yu, B. Feng, X. Geng, L. Zhang, W. Wang, and B. Shen, "Leveraging radiation reaction via laser-driven plasma fields," Plasma Phys. Controlled Fusion **61**, 065007 (2019).

[45]B. Martinez, E. d'Humières, and L. Gremillet, "Synchrotron emission from nanowire array targets irradiated by ultraintense laser pulses," New J. Phys. **60**, 074009 (2018).

[46]W. Luo, S.-D. Wu, W.-Y. Liu, Y.-Y. Ma, F.-Y. Li, T. Yuan, J.-Y. Yu, M. Chen, and Z.-M. Sheng, "Enhanced electron–positron pair production by two obliquely incident lasers interacting with a solid target," Plasma Phys. Controlled Fusion **60**, 095006 (2018).

[47]L.-Q. Zhang, S.-D. Wu, H.-R. Huang, H.-Y. Lan, W.-Y. Liu, Y.-C. Wu, Y. Yang, Z.-Q. Zhao, Z.-C. Zhu, and W. Luo, "Brilliant attosecond γ-ray emission and high-yield positron production from intense laser-irradiated nano-micro array," Phys. Plasmas **28**, 023110 (2021).

[48]R. Capdessus, L. Gremillet, and P. McKenna, "High-density electron–ion bunch formation and multi-GeV positron production via radiative trapping in extreme-intensity laser–plasma interactions," Phys. Plasmas **22**, 113003 (2020).

[49]J. Y. Yu, T. Yuan, W. Y. Liu, M. Chen, W. Luo, S. M. Weng, and Z. M. Sheng, "QED effects induced harmonics generation in extreme intense laser foil interaction," Plasma Phys. Controlled Fusion **60**, 044011 (2018).

[50]Z. Lécz and A. Andreev, "Minimum requirements for electron–positron pair creation in the interaction of ultra-short laser pulses with thin foils," Plasma Phys. Controlled Fusion **61**, 045005 (2019).

[51]Y.-J. Gu, O. Klimo, and S. Weber, "Gamma photons and electron–positron pairs from ultra-intense laser-matter interaction: A comparative study of proposed configurations," Matter Radiat. Extremes **4**, 064403 (2019).

[52]J. Q. Yu, H. Y. Lu, T. Takahashi, R. H. Hu, Z. Gong, W. J. Ma, Y. S. Huang, C. E. Chen, and X. Q. Yan, "Creation of electron–positron pairs in photon-photon collisions driven by 10-PW laser pulses," Phys. Rev. Lett. **122**, 014802 (2019).

[53]J. F. Ong, T. Moritaka, and H. Takabe, "Optimizing the energies conversion in laser–electron beam collision," Phys. Plasmas **26**, 033102 (2019).

[54]T. G. Blackburn, "Radiation reaction in electron–beam interactions with high-intensity lasers," Rev. Mod. Plasma Phys. **4**, 5 (2020).

[55]H.-Y. Zhang, L.-F. Gan, H.-B. Zhuo, B. Qiao, Y.-Y. Ma, and J.-Y. Dai, "Enhanced pair production in collisions of intense pulsed lasers with a high-energy electron beam," Phys. Rev. A **100**, 022122 (2019).

[56]M. Lobet, X. Davoine, E. d'Humières, and L. Gremillet, "Generation of high-energy electron–positron pairs in the collision of a laser-accelerated electron beam with a multipetawatt laser," Phys. Rev. Accel. Beams **20**, 043401 (2017).

[57]Z. Gong, R. H. Hu, J. Q. Yu, Y. R. Shou, A. V. Arefiev, and X. Q. Yan, "Radiation rebound and quantum splash in electron–laser collisions," Phys. Rev. Accel. Beams **22**, 093401 (2019).

[58]Y.-F. Li, Y.-Y. Chen, W.-M. Wang, and H.-S. Hu, "Production of highly polarized positron beams via helicity transfer from polarized electrons in a strong laser field," Phys. Rev. Lett. **125**, 044802 (2020).

[59]C. Slade-Lowther, D. D. Sorbo, and C. P. Ridgers, "Identifying the electron–positron cascade regimes in high-intensity laser-matter interactions," New J. Phys. **21**, 013028 (2019).

[60]Z. Gong, R. H. Hu, H. Y. Lu, J. Q. Yu, D. H. Wang, E. G. Fu, C. E. Chen, X. T. He, and X. Q. Yan, "Brilliant GeV gamma-ray flash from inverse Compton scattering in the QED regime," Plasma Phys. Controlled Fusion **60**, 044004 (2018).

[61]Y. Shi, J. Xiao, H. Qin, and N. J. Fisch, "Simulations of relativistic quantum plasmas using real-time lattice scalar QED," Phys. Rev. E **97**, 053206 (2018).

[62]A. S. Samsonov, I. Y. Kostyukov, and E. N. Nerush, "Hydrodynamical model of QED cascade expansion in an extremely strong laser pulse," Matter Radiat. Extremes **6**, 034404 (2021).

[63]A. R. Bell and J. G. Kirk, "Possibility of prolific pair production with high-power lasers," Phys. Rev. Lett. **101**, 200403 (2008).

[64]A. M. Fedotov, N. B. Narozhny, G. Mourou, and G. Korn, "Limitations on the attainable intensity of high power lasers," Phys. Rev. Lett. **105**, 080402 (2010).

[65]S. S. Bulanov, T. Z. Esirkepov, A. G. R. Thomas, J. K. Koga, and S. V. Bulanov, "Schwinger limit attainability with extreme power lasers," Phys. Rev. Lett. **105**, 220407 (2010).

[66]E. N. Nerush, I. Y. Kostyukov, A. M. Fedotov, N. B. Narozhny, N. V. Elkina, and H. Ruhl, "Laser field absorption in self-generated electron–positron pair plasma," Phys. Rev. Lett. **106**, 035001 (2011).

[67]N. V. Elkina, A. M. Fedotov, I. Y. Kostyukov, M. V. Legkov, N. B. Narozhny, E. N. Nerush, and H. Ruhl, "QED cascades induced by circularly polarized laser fields," Phys. Rev. Spec. Top. Accel. Beams **14**, 054401 (2011).

[68]M. Jirka, O. Klimo, S. V. Bulanov, T. Z. Esirkepov, E. Gelfer, S. S. Bulanov, S. Weber, and G. Korn, "Electron dynamics and γ and $e^- e^+$ production by colliding laser pulses," Phys. Rev. E **93**, 023207 (2016).

[69]T. Grismayer, M. Vranic, J. L. Martins, R. A. Fonseca, and L. O. Silva, "Laser absorption via quantum electrodynamics cascades in counter propagating laser pulses," Phys. Plasmas **23**, 056706 (2016).

[70]X.-L. Zhu, T.-P. Yu, Z.-M. Sheng, Y. Yin, I. C. E. Turcu, and A. Pukhov, "Dense GeV electron–positron pairs generated by lasers in near-critical-density plasmas," Nat. Commun. **7**, 13686 (2016).

[71]M. Tamburini, A. D. Piazza, and C. H. Keitel, "Laser-pulse-shape control of seeded QED cascades," Sci. Rep. **7**, 5694 (2017).

[72]A. Gonoskov, A. Bashinov, S. Bastrakov, E. Efimenko, A. Ilderton, A. Kim, M. Marklund, I. Meyerov, A. Muraviev, and A. Sergeev, "Ultrabright GeV photon source via controlled electromagnetic cascades in laser-dipole waves," Phys. Rev. X **7**, 041003 (2017).

[73]T. Grismayer, M. Vranic, J. L. Martins, R. A. Fonseca, and L. O. Silva, "Seeded QED cascades in counterpropagating laser pulses," Phys. Rev. E **95**, 023210 (2017).

[74]A. F. Savin, A. J. Ross, R. Aboushelbaya, M. W. Mayr, B. Spiers, R. H.-W. Wang, and P. A. Norreys, "Energy absorption in the laser-QED regime," Sci. Rep. **9**, 8956 (2019).

[75]K. Qu, S. Meuren, and N. J. Fisch, "Signature of collective plasma effects in beam-driven QED cascades," Phys. Rev. Lett. **127**, 095001 (2021).

[76]E. Cartlidge, "The light fantastic," Science **359**, 382 (2018).

[77]J. Bromage, S.-W. Bahk, I. A. Begishev, C. Dorrer, M. J. Guardalben, B. N. Hoffman, J. Oliver, R. G. Roides, E. M. Schiesser, M. J. Shoup III et al., "Technology development for ultraintense all-OPCPA systems," High Power Laser Sci. **7**, e4 (2019).

[78]C. N. Danson, C. Haefner, J. Bromage, T. Butcher, J.-C. Chanteloup, E. A. Chowdhury, A. Galvanauskas, L. A. Gizzi, J. Hein, D. I. Hillier et al., "Petawatt and exawatt class lasers worldwide," High Power Laser Sci. Eng. **7**, e54 (2019).

[79]V. Yakimenko, L. Alsberg, E. Bong, G. Bouchard, C. Clarke, C. Emma, S. Green, C. Hast, M. J. Hogan, J. Seabury, N. Lipkowitz, B. O'Shea, D. Storey, G. White, and G. Yocky, "FACET-II facility for advanced accelerator experimental tests," Phys. Rev. Accel. Beams **22**, 101301 (2019).

[80]C. Bula, K. T. McDonald, E. J. Prebys, C. Bamber, S. Boege, T. Kotseroglou, A. C. Melissinos, D. D. Meyerhofer, W. Ragg, D. L. Burke, R. C. Field, G. Horton-Smith, A. C. Odian, J. E. Spencer, D. Walz et al., "Observation of nonlinear effects in Compton scattering," Phys. Rev. Lett. **76**, 3116 (1996).

[81]D. L. Burke, R. C. Field, G. Horton-Smith, J. E. Spencer, D. Walz, S. C. Berridge, W. M. Bugg, K. Shmakov, A. W. Weidemann, C. Bula, K. T. McDonald, E. J. Prebys, C. Bamber, S. J. Boege, T. Koffas et al., "Positron production in multiphoton light-by-light scattering," Phys. Rev. Lett. **79**, 1626 (1997).

[82]G. White and V. Yakimenko, "On possible upgrades to FACET-II," personal communication (2020).

[83]G. White and V. Yakimenko, "Ultra-short-z linear collider parameters," arXiv:1811.11782 (2018).

[84]V. Yakimenko, S. Meuren, F. Del Gaudio, C. Baumann, A. Fedotov, F. Fiuza, T. Grismayer, M. J. Hogan, A. Pukhov, L. O. Silva, and G. White, "Prospect of studying nonperturbative QED with beam–beam collisions," Phys. Rev. Lett. **122**, 190404 (2019).

[85]S. C. Wilks, J. M. Dawson, and W. B. Mori, "Frequency up-conversion of electromagnetic radiation with use of an overdense plasma," Phys. Rev. Lett. **61**, 337 (1988).

[86]E. Esarey, A. Ting, and P. Sprangle, "Frequency shifts induced in laser pulses by plasma waves," Phys. Rev. A **42**, 3526 (1990).

[87]W. M. Wood, C. W. Siders, and M. C. Downer, "Measurement of femtosecond ionization dynamics of atmospheric density gases by spectral blue-shifting," Phys. Rev. Lett. **67**, 3523 (1991).

[88]K. Qu and N. J. Fisch, "Laser frequency upconversion in plasmas with finite ionization rates," Phys. Plasmas **26**, 083105 (2019).

[89]M. R. Shcherbakov, K. Werner, Z. Fan, N. Talisa, E. Chowdhury, and G. Shvets, "Photon acceleration and tunable broadband harmonics generation in nonlinear time-dependent metasurfaces," Nat. Commun. **10**, 1345 (2019).

[90]A. Nishida, N. Yugami, T. Higashiguchi, T. Otsuka, F. Suzuki, M. Nakata, Y. Sentoku, and R. Kodama, "Experimental observation of frequency upconversion by flash ionization," Appl. Phys. Lett. **101**, 161118 (2012).

[91]K. Qu, Q. Jia, M. R. Edwards, "Theory of electromagnetic wave frequency upconversion in dynamic media," Phys. Rev. E **98**, 023202 (2018).

[92]M. R. Edwards, K. Qu, Q. Jia, J. M. Mikhailova, and N. J. Fisch, "Cascaded chirped photon acceleration for efficient frequency conversion," Phys. Plasmas **25**, 053102 (2018).

[93]S. S. Bulanov, A. M. Fedotov, and F. Pegoraro, "Damping of electromagnetic waves due to electron–positron pair production," Phys. Rev. E **71**, 016404 (2005).

[94]H. Peng, C. Riconda, S. Weber, C. T. Zhou, and S. C. Ruan, "Frequency conversion of lasers in a dynamic plasma grating," Phys. Rev. Appl. **15**, 054053 (2021).

[95]R. G. Greaves and C. M. Surko, "An electron–positron beam-plasma experiment," Phys. Rev. Lett. **75**, 3846 (1995).

[96]B. D. Fried, "Mechanism for instability of transverse plasma waves," Phys. Fluids **2**, 337 (1959).

[97]M. R. Edwards, N. J. Fisch, and J. M. Mikhailova, "Strongly enhanced stimulated Brillouin backscattering in an electron–positron plasma," Phys. Rev. Lett. **116**, 015004 (2016).

[98]V. B. Berestetskii, E. M. Lifshitz, and L. P. Pitaevskii, *Quantum Electrodynamics*, 2nd ed. (Butterworth-Heinemann, 1982).

[99]M. Aicheler, P. Burrows, M. Draper, T. Garvey, P. Lebrun, K. Peach, N. Phinney, H. Schmickler, D. Schulte, and N. Toge, *A Multi-TeV Linear Collider Based on CLIC Technology: CLIC Conceptual Design Report*, CERN Yellow Reports: Monographs (CERN, Geneva, 2012).

[100]A. Caldwell, K. Lotov, A. Pukhov, and F. Simon, "Proton-driven plasma-wakefield acceleration," Nat. Phys. **5**, 363 (2009).

[101]T. D. Arber, K. Bennett, C. S. Brady, A. Lawrence-Douglas, M. G. Ramsay, N. J. Sircombe, P. Gillies, R. G. Evans, H. Schmitz, A. R. Bell et al., "Contemporary particle-in-cell approach to laser-plasma modelling," Plasma Phys. Controlled Fusion **57**, 113001 (2015).

[102]C. P. Ridgers, J. G. Kirk, R. Duclous, T. G. Blackburn, C. S. Brady, K. Bennett, T. D. Arber, and A. R. Bell, "Modelling gamma-ray photon emission and pair production in high-intensity laser–matter interactions," J. Comput. Phys. **260**, 273 (2014).

[103]J.-X. Li, K. Z. Hatsagortsyan, B. J. Galow, and C. H. Keitel, "Attosecond gamma-ray pulses via nonlinear compton scattering in the radiation-dominated regime," Phys. Rev. Lett. **115**, 204801 (2015).

[104]D. J. Kane and R. Trebino, "Characterization of arbitrary femtosecond pulses using frequency-resolved optical gating," IEEE J. Quantum Electron. **29**, 571 (1993).

[105]C. Iaconis and I. A. Walmsley, "Spectral phase interferometry for direct electric-field reconstruction of ultrashort optical pulses," Opt. Lett. **23**, 792 (1998).

[106]A. J. Gonsalves, K. Nakamura, J. Daniels, C. Benedetti, C. Pieronek, T. C. H. de Raadt, S. Steinke, J. H. Bin, S. S. Bulanov, J. van Tilborg, C. G. R. Geddes, C. B. Schroeder, C. Tóth, E. Esarey, K. Swanson, L. Fan-Chiang, G. Bagdasarov, N. Bobrova, V. Gasilov, G. Korn, P. Sasorov, and W. P. Leemans, "Petawatt laser guiding and electron beam acceleration to 8 GeV in a laser-heated capillary discharge waveguide," Phys. Rev. Lett. **122**, 084801 (2019).

[107]S. Meuren, P. H. Bucksbaum, N. J. Fisch, F. Fiúza, S. Glenzer, M. J. Hogan, K. Qu, D. A. Reis, G. White, and V. Yakimenko, "On seminal HEDP research opportunities enabled by colocating multi-petawatt laser with high-density electron beams," arXiv:2002.10051 (2020).

[108]S. Meuren, D. A. Reis, R. Blandford, P. H. Bucksbaum, N. J. Fisch, F. Fiuza, E. Gerstmayr, S. Glenzer, M. J. Hogan, C. Pellegrini, M. E. Peskin, K. Qu, G. White, and V. Yakimenko, "MP3 white paper 2021—Research opportunities enabled by co-locating multi-petawatt lasers with dense ultra-relativistic electron beams," arXiv:2105.11607 (2021).